

Fatigue Crack Initiation and Propagation in Superalloy IN 713LC

L. Kunz¹, P. Lukáš¹ and R. Konečná²

¹ Institute of Physics of Materials, AS CR, Žitkova 22, 616 62 Brno, Czech Republic.
e-mail: kunz@ipm.cz.

² Žilina University, Department of Materials Engineering, Univerzitná 1, Slovak Republic. e-mail: radomila.konecna@fstroj.uniza.sk

ABSTRACT. *High-cycle fatigue life of cast Ni-base superalloy IN 713LC under load symmetrical cycling and cycling with tensile mean stress was experimentally determined. The fatigue life exhibits very large scatter. Both crystallographic Stage I crack propagation and non-crystallographic Stage II propagation were observed. High scatter of fatigue life data was explained by (i) variability in microstructural conditions for crystallographic crack initiation and propagation and by (ii) influence of casting defect size distribution. The fractographic observation supports the slip band decohesion model for crack initiation and early crack propagation and important role of cyclic slip localization in persistent slip bands.*

INTRODUCTION

High-cycle fatigue (HCF) performance of engineering materials is closely related to fatigue crack initiation and early crack propagation. These two periods of fatigue cracking often represent the decisive part of fatigue lifetime. Both the crack initiation and early crack propagation are highly sensitive to material microstructure. In most crystalline metals and alloys fatigue crack initiation occurs along crystallographic slip planes at an external surface [1]. This mode of cracking has been called Stage I. The corresponding fatigue fracture surface (or fatigue crack length) is usually small and limited to one surface grain. Crack propagation in the Stage I takes place along slip planes of high resolved shear stress. It is controlled by the shear component of the applied stress. The crack length at which the propagation mode changes from the Stage I to the non-crystallographic Stage II depends mainly on material, temperature and the stress amplitude.

Ni-base superalloys are f.c.c. with slip systems $\{111\} \langle 110 \rangle$. Deformation occurs heterogeneously in planar bands lying along the crystallographic planes $\{111\}$ and, as a result, extensive very long Stage I cracking is observed. Antolovich [2] summarizes that crystallographic Stage I crack propagation has been observed in both single crystal and polycrystal nickel-base superalloys. The extent of crystallographic crack propagation appears to be influenced by temperature [3], environment and frequency [4] and in the

case of long cracks by stress intensity factor amplitude K_a [5, 6]. In the case of notches in Ni-base alloys, the fatigue cracks initiate at the slip bands in the plastic zone which provide favourable sites for crack imitation and propagation [7].

Conventionally cast Ni-base superalloy IN 713LC is an engineering material, which has been used in turbine industry since the fifties of the last century. Surprisingly, the high-cycle high temperature fatigue life data are quite rare in the open literature. The knowledge on the influence of mean stress on fatigue behaviour is even more limited [8]. A typical feature of HCF strength of cast superalloys is high scatter of life data. This effect can be attributed to casting defects, microshrinkages and other inhomogeneities, which are sites of crack initiation. Their influence can be diminished by hot isostatic pressing technology. Its beneficial effect on fatigue performance was reported [9], but the results often fall short of expectations. In the case of materials exhibiting different modes of fatigue crack initiation and early crack propagation one of the reasons of the large scatter may be the variability of conditions for crack initiation and early propagation.

This work is focused on investigation of HCF crack initiation, propagation and fatigue life of conventionally cast superalloy IN 713LC loaded at 800 °C in air in symmetrical cycle and in asymmetrical cycle with tensile mean stresses 300 and 400 MPa. The aim is to discuss and explain the scatter of fatigue life data in terms of crack initiation and propagation mechanisms and to obtain more information concerning the influence of microstructure on fatigue damage.

MATERIAL AND EXPERIMENTS

Conventionally cast rods of IN 713LC having 20 mm in diameter and 100 mm in length were used for manufacturing of specimens. The chemical composition of the alloy is given in Tab.1. All rods were controlled by conventional x-ray defectoscopy with the resolution limit of 0.5 mm. They were found “defect free” in this sense.

Table 1. Chemical composition of IN 713LC superalloy (wt. %)

C	Mn	Si	Cr	Ti	Al	Fe	B	Zr	Nb	Ta	Mo	Co	Cu	P	S	Ni
0.007	<0.05	0.06	11.63	0.77	5.91	0.18	0.12	0.12	2.36	0.09	4.66	0.30	<0.05	0.007	0.004	Bal.

The microstructure of cast IN 713LC is of dendritic nature. An example of a structure in transversal section of a cast rod is shown in Fig. 1. The microstructure at higher magnification can be seen in Fig. 2. The dendritic regions are characteristic by fine and homogeneous γ/γ' structure. In the interdendritic regions colonies of large γ' particles, carbides and casting defects are present.

Casting defects as observed on polished axial metallographical section of the gauge length of a specimen are shown in Fig. 3. Their distribution is not uniform. They are

sometimes grouped and form clusters. In three-dimensional space the defects form interconnected systems.

Cylindrical button end specimens for fatigue tests, Fig. 4, having 5 mm in diameter and 35 mm gauge length were machined from the cast rods.

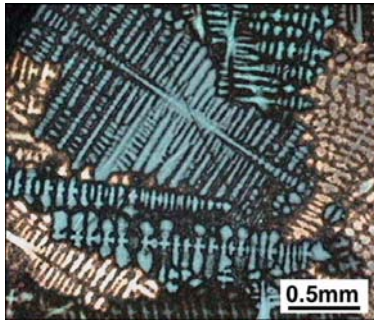


Figure 1. Dendritic structure in transversal section.

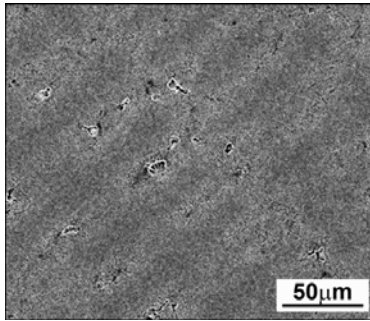


Figure 2. γ/γ' structure in transversal section.

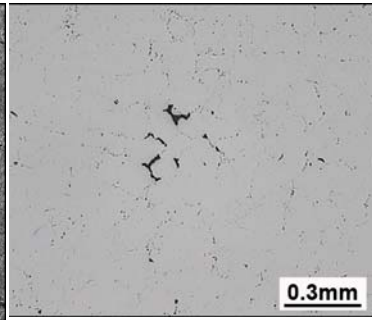


Figure 3. Casting defects.

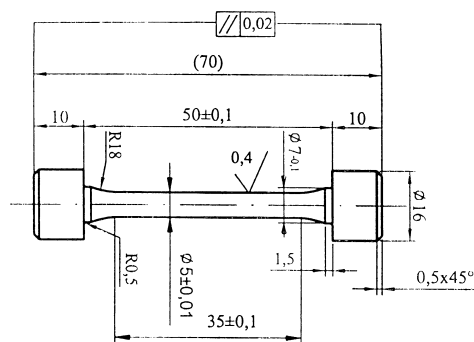


Figure 4. Specimen for fatigue tests.

Fatigue tests were performed at 800 °C in laboratory air at controlled load in a 100 kN resonant testing machine. The frequency of sine wave loading was 105 ± 3 Hz. The start-up procedure of a test consisted of heating up the specimen at controlled zero stress. One hour after the desired temperature was reached the mean stress has been applied within some seconds and subsequently the resonant system was switched on. The load amplitude was reached during a ramp of a length of about 500 cycles.

RESULTS

Experimentally determined fatigue life for loading with zero mean stress and with tensile mean stresses $\sigma_{\text{mean}} = 300$ and 400 MPa is shown in Fig. 5. The open points with arrows indicate run out specimens. The following conclusions can be drawn from the results: The increase of tensile mean stress from 0 to 300 MPa results in a considerable shift of S-N points to lower stress amplitudes. Further increase of σ_{mean} to 400 MPa has weaker effect. The S-N data in Fig. 5 exhibit very large scatter. In the case of the stress symmetrical loading at the stress amplitude 180 MPa, one specimen failed at 6.5×10^4 cycles, whereas another specimen at the same stress amplitude level did not fail after 2.5×10^7 cycles, which is a difference of more than 3 orders in magnitude. Similar scatter can be observed for loading with mean stresses.

Two types of fatigue crack initiation and propagation were recognized on fracture surfaces of failed specimens. The first type is shown in Fig. 6 and corresponds to the loading with $\sigma_{\text{mean}} = 300$ MPa and stress amplitude $\sigma_a = 120$ MPa. The crack starts

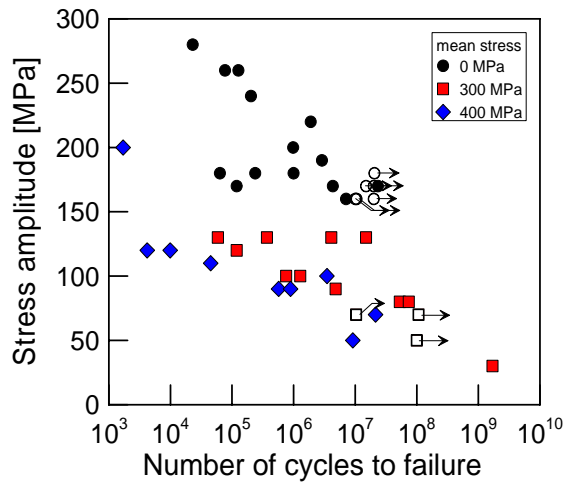


Figure 5. S-N data of IN 713LC for $\sigma_{\text{mean}} = 0$, 300 and 400 MPa, 800 °C.

obviously from a large internal casting defect. The macroscopic crack plane is nearly perpendicular to the principal stress. Large “fish eye” surrounding the defect is visible on the fracture surface. There are distinct traces of macroscopic features of dendritic structure on the fracture surface within the fish eye. The crack surface appearance suddenly changed when the crack reached the surface of the specimen and the laboratory atmosphere interfered with the freshly created fracture surface. The near vicinity of the casting defect in another specimen with similar failure is shown in

Fig. 7. The fracture surface is again of non-crystallographic type. The dendritic structure, coarse γ' precipitates and small casting porosity in interdendritic regions can

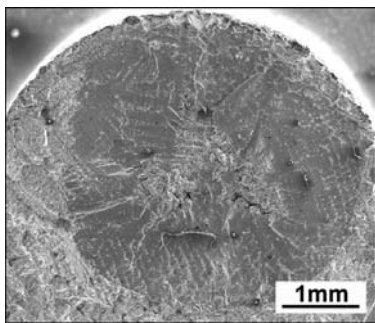


Figure 6. Fish eye on fracture surface.

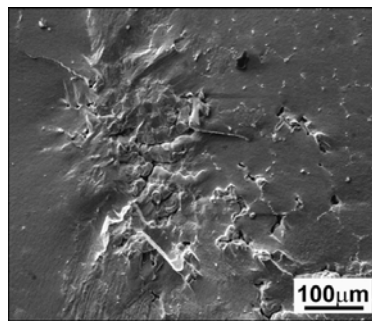


Figure 7. Fracture surface in the vicinity of casting defect.

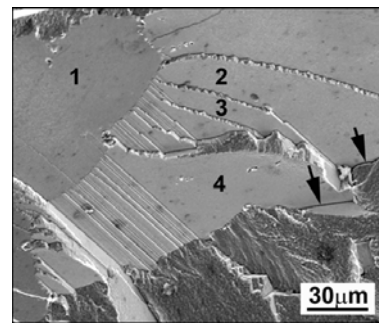


Figure 8. Crystallographic facets on fracture surface.

be identified, see right upper corner in Fig. 7. The second type of crack initiation and early crack propagation is shown in Fig. 8. The fracture surface corresponds to the specimen loaded at $\sigma_{\text{mean}} = 300$ MPa and $\sigma_a = 130$ MPa. Systems of plain crystallographic facets can be seen. They are mutually inclined at high angles; in Fig 8 this holds for facet marked as 1 and facets 2, 3 and 4. On the other hand, facets marked by 2, 3 and 4 belong to one parallel system. At low magnification, as observed by light microscopy, the facets have high reflexivity and mirror like appearance. At high

magnification decohesion of material along the facets can be often observed. Arrows in Figs. 8 and 9 denote the sites of decohesion. The direction of observation in Fig. 9 was chosen in such a way that the facet on the right hand side was at low angle to the direction of observation and the facet on the left hand side was nearly perpendicular

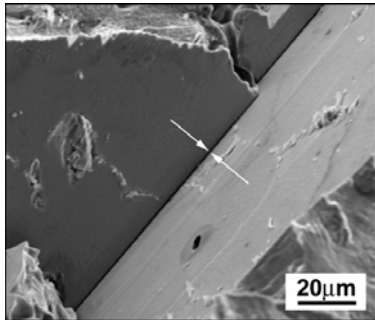


Figure 9. Decohesion of crystallographic facets. Arrows mark the distance between facets.

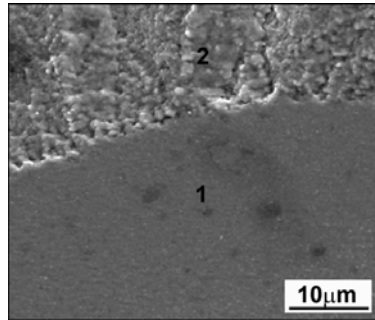


Figure 10. Fracture surface of a facet (1) and surface corresponding to non-crystallographic crack propagation (2).

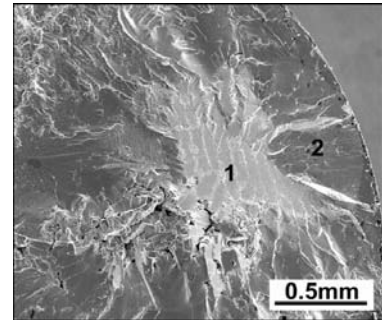


Figure 11. Crystallographic facet (1) near a casting defect. Non-crystallographic fracture surface (2).

to the direction of observation. Under this conditions decohesion of both facets marked by two arrows is well recognizable. Transition of a crystallographic facet to non-crystallographic propagation is shown in Fig. 10. The surface denoted as 1 corresponds to the crystallographic facet. The surface is very smooth when compared to the region of the non-crystallographic propagation, denoted as region 2 (the upper part of the Figure). The characteristic dimension of roughness of non-crystallographic surface corresponds to the characteristic dimension of the fine γ/γ' structure.



Figure 12. Crystallographic facets on the fracture profile. Axial section through the fracture surface.

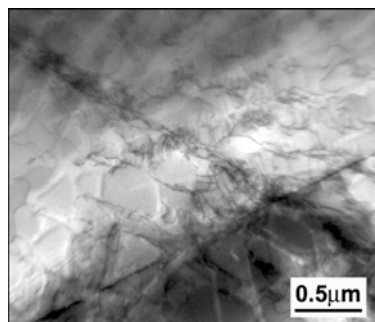


Figure 13. Intersecting planar slip bands in a specimen loaded at $\sigma_{\text{mean}} = 300 \text{ MPa}$ and $\sigma_a = 130 \text{ MPa}$.

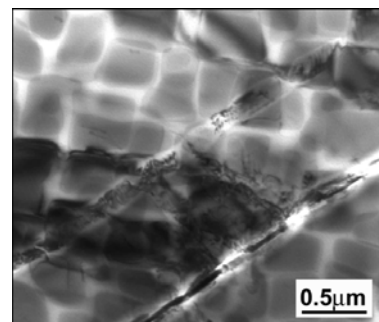


Figure 14. Parallel well developed slip bands intersecting the γ/γ' structure.

The crystallographic facets often develop near large casting defects. An example is shown in Fig. 11. The crystallographic facet is marked as surface 1 and the connecting

non-crystallographic fracture surface as 2. However, in some cases no casting defects occur in the neighbourhood of facets.

An axial section of a specimen gauge length through the fracture surface is shown in Fig. 12. Arrows mark the crystallographic facets. They intersect the dendritic structure without any evidence of being deflected by it. The traces of facet planes on metallographic section are straight. Further, it can be seen that the facets terminate at the grain boundaries. Connecting non-crystallographic fatigue fracture surface has substantially higher roughness.

Dislocation structure of fatigued IN 713LC with tensile mean stress as observed by transmission electron microscopy (TEM) is shown in Figs. 13 and 14. Intensive planar slip bands intersect the γ/γ' structure. The bands are very thin and in some cases they seem to be cracked.

DISCUSSION

Ni-base superalloys exhibit low stacking fault energy, which makes the cross-slip difficult. This expresses itself by planar deformation and by development of intense cyclic slip bands. Highly inhomogeneous dislocation arrangement was observed by Petrevec et al. [10] in IN 713LC, loaded at 800 °C. Planar arrangements in the form of bands parallel to the $\{111\}$ planes develop at low-cycle fatigue (LCF) loading under controlled strain. The bands appear as thin slabs of high dislocation density cutting both the γ channels and γ' precipitates. The presence of mean stress influences the development of slip bands in Ni-base alloys. LCF at 850 °C does not produce the slip bands in Ni-base superalloy single crystals CMSX-4 [11], whereas addition of small cyclic component to large static stress leads to formation of slip bands [12]. From Fig. 13 and 14 it is obvious that the high dislocation density slip bands in IN 713LC form at 800 °C under presence of tensile mean stresses in HCF region. The foil was prepared from a specimen which failed after loading with $\sigma_{\text{mean}} = 300$ MPa and $\sigma_a = 130$ MPa after 1.5×10^7 cycles. Fig. 14 shows the slip bands, which look like cracked. It cannot be excluded that the slots in bands come from more intense etching of highly deformed areas when the foil was prepared. Nevertheless, it seems to be a strong witness of the fact that the bands are “weakened” volumes in material. The observation of crystallographic facets on fracture surfaces demonstrates decohesion between facets, Figs. 8 and 9. The neighbouring facets are mutually fully separated. The separation distance is of some microns and is of the same extent over the whole facet.

As regards the mode of crack propagation in Ni-base polycrystals and single crystals there is a general agreement that both the crystallographic Stage I and the non-crystallographic Stage II take place and that their occurrence is a function of temperature, environment, frequency of loading and the crack growth rate. The majority of studies was performed on long cracks, e.g. [6, 13]. The detailed mechanisms of crack growth in both stages is not completely clear though the general features of fatigue crack propagation in f.c.c. metals were summarized many years ago [14]. For Ni-base single crystals Duquette et al. [15] proposed a decohesion model based on weakening of

slip planes coplanar with the crack tip. Subsequent failure, starting at a surface-connected pore proceeds by a combination of local normal and shear stress. The crack propagates along the {111} crystallographic plane. The decohesion model considers a continuous crack growth along the slip plane with increasing crack length. Our observation of decohesion of facets combined with observation of weakened slip bands by TEM indicates an alternative mechanism: HCF loading develops “weak” slip bands intersecting the whole grain, along which the material separates due to cyclic slip on non-coplanar slip systems in neighbouring grains. The occurrence of uniformly separated surfaces along the slip planes, Fig. 9 supports this alternative mechanism.

Irrespective of the details of the mechanism of decohesion, after sufficiently high number of loading cycles interior internal cracks along {111} planes develop. Their dimension and orientation depends on the variability of microstructure and the grain size of particular specimen. Planar cracks, which are inclined at various angles to the loading direction, once developed, serve later on in the fatigue process as starters of the final crack, which propagates internally by the non-crystallographic Stage II and forms the fish eye, Fig. 11. The number of cycles necessary to the development of planar cracks varies according to the particular microstructural conditions. Because the stress intensity factors are different subsequent crack growth can differ in crack propagation rate. The final impact is scatter in HCF lifetime.

From the fractographic analysis it is evident that facets can be often found in areas adjacent to large casting defects, which form interconnected systems. The reason for it is their stress concentration effect. They increase the local stress amplitude, promote the slip on adjacent slip planes and contribute to the decohesion process. The defects contribute to the scatter of fatigue life data in this way because they have different stress concentration factor due to their different shape.

The distribution of casting defects is probabilistic, which means that in some specimens extraordinary large defects or their agglomerates can occur. They initiate cracks due to their stress concentration effect in similar way as the small ones. However, once the crack is initiated at a large defect, it propagates with a rate determined by the stress intensity factor amplitude K_a corresponding to the crack length including the defect dimension. If this is of the order of some tens of millimetres, the K_a value may be sufficiently high to promote the Stage II propagation from the very beginning. This is the case shown in Fig. 6. The loading parameters were the following: $\sigma_{\text{mean}} = 300$ MPa, $\sigma_a = 120$ MPa and the number of cycles to failure 1.19×10^5 . On the other hand, at the same mean stress, at even a slightly higher stress amplitude $\sigma_a = 130$ MPa, but in the absence of a large casting defect, the crystallographic initiation and propagation by Stage I took place, Fig. 8, which resulted in more than one order of magnitude higher number of cycles to failure, namely 4.1×10^6 .

CONCLUSIONS

1. Tensile mean stresses of 300 and 400 MPa reduce the high-cycle fatigue strength of IN 713LC alloy at 800 °C when compared to the symmetrical loading. The S-N data exhibit a scatter more than three orders of magnitude.

2. Fatigue fracture surface is either non-crystallographic, corresponding to the Stage II crack propagation or crystallographic, corresponding to the Stage I cracking. Both types of crack propagation can be found in a broad interval of mean stresses and stress amplitudes.
3. Casting defects play an important role in fatigue crack initiation and early propagation.
4. High scatter of fatigue life can be explained by (i) variability of microstructural conditions for development of slip bands and related crystallographic crack initiation and (ii) by the influence of casting defect size distribution.

ACKNOWLEDGEMENT

This work was supported by the project FT/TA4/023 of the Ministry of Industry and Trade of the Czech Republic and the project 1QS200410502 of the Academy of Sciences of the Czech Republic. This support is gratefully acknowledged.

REFERENCES

1. Klesnil, M. and Lukáš, P. (1992) *Fatigue of Metallic Materials*. Academia/Elsevier Prague.
2. Antolovich, B.F. (1996). In: *ASM Handbook Fatigue and Fracture*. Vol. 19. ASM Int. pp. 884-868.
3. Chu, Z., Yu, J., Sun, X., Guan, H. and Hu, Z. (2008) *Mat. Sci. Eng. A* **496**, 355-361.
4. Leverant, G.R. and Gell M. (1975) *Met. Trans.* **6A**, 367-371.
5. Yu, W., Yuan, J. and Wang, Z. (1987) *Fatigue Fract. Engng. Mater. Struct.* **9**, 425-434.
6. King, J.E. (1987) *Mater. Sci. Technol.* **3**, 750-764.
7. Ren, W. and Nicholas, T. (2003) *Mat. Sci. Eng. A* **357** 141-152.
8. Kunz, L., Lukáš, P., Mintách, R. and Hrbáček, K. (2006) *Kovove Mater.* **44**, 275-281.
9. Donachie, M.J. and Donachie, S.J. (2002). *Superalloys. A Technical Guide*. 2nd Edition. ASM Int.
10. Petrevec, M., Obrtlík, K. and Polák, J. (2005) *Mat. Sci. Eng. A* **400-401**, 485-488.
11. Obrtlík, K., Lukáš, P. and Polák, J. (1998) In: *Low Cycle Fatigue and Elasto-Plastic Behaviour of Materials*. Rie, K.T. and Portella P.D. eds. Elsevier, 33-38.
12. Lukáš, P., Kunz, L. and Svoboda M. (2004) *Mater. Sci. Eng. A* **387-389**, 505-510.
13. Crompton, J.S. and Martin J.W. (1984) *Met. Trans.* **15A**, 1711-1719.
14. McEvily, A.J.Jr. and Boettner R.C. (1963) *Acta Metallurgica* **11**, 725-743.
15. Duquette, D.J., Gell, M. and Pietsch, J. W. (1970) *Met. Trans.* **1**, 3107-3115.